Articles

H2O2 Generation at a Carbon-Paste Electrode with Decamethylferrocene in 2-Nitrophenyloctyl Ether as a Binder: Catalytic Effect of MoS2 Particles

Justyna Jedraszko,[a] Olga Krysiak,[a] Wojciech Adamiak,[a] Wojciech Nogala,[a] Hubert H. Girault,[b] and Marcin Opallo*[a]

Here, we report hydrogen peroxide generation at the 2-nitrophenyloctyl ether (NPOE)/water interface with decamethylferrocene as an electron donor. The progress of this reaction was detected by the observation of a color change in the organic and aqueous phases in a series of shake-flask experiments. The shape change in cyclic voltammograms recorded at a carbon-paste electrode with decamethylferrocene in NPOE also indicates a (electro)catalytic reaction. Hydrogen peroxide was electrochemically detected at a Pt microelectrode tip positioned next to the carbon-paste electrode. For this purpose, scanning electrochemical microscopy (SECM) approach curves were recorded. Analogous experiments demonstrated the possibility of electrochemical regeneration of the electron donor. The (electro)catalytic effect of MoS2 on hydrogen peroxide generation was found by using both shake-flask and SECM experiments.

1. Introduction

Formation of simple chemicals, like hydrogen peroxide, at soft interfaces between two immiscible electrolyte solutions (ITIES) has gained an increasing attention over the last several years.[1–3] This is because these reactions can be driven by polarization of the liquid–liquid interface. In practice, this can be done by applying external voltage or by appropriate selection of electrolytes with a common ion in both liquid phases.[1,4] Also, the existence of two liquid phases in contact allows separation of the reactants and/or catalysts, which can be beneficial for both the efficiency and selectivity of the reaction.

Hydrogen peroxide is produced on a large scale by catalytic hydrogenation and oxidation of the alkylanthraquinone precursor dissolved in an organic solvent mixture, followed by the extraction of the product from the organic to the aqueous phase.[5,6] Application of liquid–liquid interface for this process is an interesting alternative. For this purpose, molecular solvents like 1,2-dichloroethane,[7] 1,2-dichlorobenzene,[8] and trifluorotoluene[9] have been used as water-immiscible organic media. It has been demonstrated that H2O2 is formed in a two-electron reduction of oxygen by a hydrophobic electron donor (metallocene) dissolved in the organic solvent with simultaneous access to protons from the aqueous phase.[10] The reaction occurs either under conditions favorable for proton transfer from the aqueous phase to the organic phase[10] or when the potential drop across the liquid–liquid interface is not favorable,[11] which includes systems without deliberately added electrolyte in the organic phase.[12] Under conditions favorable for proton transfer to the organic phase, H2O2 generation involves homogeneous electron transfer within the bulk organic phase, whereas under unfavorable conditions heterogeneous electron transfer at the liquid–liquid interface is a dominant process.[10–12]

Independent of the reaction mechanism (homogeneous or heterogeneous ET), the oxidized decamethylferrocene is not transferred to the aqueous phase.[7–12] This creates a possibility of electrochemical regeneration of the electron donor in the bulk organic solution. To perform noticeable regeneration, one can confine the organic phase to a small volume and immobilize it on an electrode surface. It is crucial that the organic phase is stable over time, which limits the choice of the water-immiscible solvents to nonvolatile ones, for example viscous ionic liquids. Recently, we have found that the constituent ions of the ionic liquid can also be transferred to water during the two-phase reaction.[13] This behavior can lead to gradual dissolution of the organic liquid and is highly undesirable in terms of electrochemical regeneration and stability of the system in general. In this respect, much better candidates seem to be nonvolatile water-immiscible molecular solvents because their neutral molecules are not transferred during the reaction.

Herein, we describe the use of viscous 2-nitrophenyloctyl ether (NPOE) as a suitable nonvolatile water-immiscible solvent for generation of hydrogen peroxide and electrochemical regeneration of the electron donor. To provide favorable conditions for the regeneration, we used a carbon-paste electrode (CPE) composed of the viscous solvent and graphite particles.[14] This architecture allows us to overcome mass-transport limitations caused by the high viscosity of the solvent and pro-

[a] J. Jedraszko, O. Krysiak, Dr. W. Adamiak, Dr. W. Nogala, Prof. M. Opallo
Institute of Physical Chemistry, Polish Academy of Sciences
Kasprzaka 44/52, 01-224 Warsaw (Poland)
E-mail: mopallo@ichf.edu.pl

[b] Prof. H. H. Girault
EPFL Valais Wallis, EPFL SB ISIC LEPA
Rue de l'Industrie 17, Case postale 440, CH-1951 Sion (Switzerland)

Supporting Information for this article can be found under:
http://dx.doi.org/10.1002/celc.201600242.

1400

vides suitable conditions for organic-phase immobilization. It can also be considered as a simple platform for testing the catalytic properties of solid particles in the studied processes because it allows us to overcome problems with particle adsorption, aggregation, or sedimentation. Taking advantage of these properties, we also used the CPE to investigate the possible catalytic effect of MoS_2 particles on H_2O_2 generation at an NPOE/water interface. The use of various nanomaterials as catalysts for the liquid–liquid oxygen reduction reaction (ORR) or hydrogen evolution reaction (HER) has been extensively studied over the last few years,[15–19] but none of them have been applied to an NPOE/water interface system.

Although the electrocatalytic activity of MoS_2 towards ORR at solid–liquid interface has been reported previously,[20, 21] it has not been tested at a liquid–liquid interface. However, this material is already known to be a catalyst for HER at the liquid–liquid interface.[22, 23] Here, we examine MoS_2 as a catalyst for the liquid–liquid ORR with a particular focus on electrochemical regeneration of the electron donor. For this purpose, scanning electrochemical microscopy (SECM) was employed. This method has been used previously to probe charge-transfer processes at ITIES, such as heterogeneous electron transfer across a "clear" interface[24, 25] or a molecular monolayer.[26, 27] Other reactions include facilitated[28] or simple ion transfer,[29] and processes with coupled homogeneous reactions at ITIES.[30] We also investigated the influence of MoS_2 on the ion-transfer processes driven by electrogenerated redox-active ions[31–34] because H_2O_2 generation at ITIES is an ion-transfer-coupled reaction.[10]

2. Results and Discussion

2.1. Flask Experiments

NPOE has not been used to date as a water-immiscible solvent for the two-phase generation of H_2O_2. Therefore, we performed shake-flask experiments to find whether formation of H_2O_2 occurs in the NPOE/water system (Figure 1).

It is clearly visible that after 8 h, the color of NPOE phase in contact with the acidic aqueous solution has changed from yellow to green, which indicates the formation of $DMFc^+$ cations (Figure 1 A, B, flask 1). This change is not seen in the absence of acid in the aqueous phase (Figure 1 A, B, flask 2), which indicates the participation of hydrated protons in the two-phase reaction. When NPOE is in contact with the acidic solution, the change in color is even more pronounced in the presence of MoS_2 particles (Figure 1 A, B, flask 3), which demonstrates their catalytic activity in this reaction. It is also important to emphasize that these color changes are not seen under anaerobic conditions, which indicates negligible formation of hydrogen in studied system.[15–19] The progress of reaction was also followed by UV/Vis spectroscopy (Figure 2 A) One can see a decrease in the band at $\lambda = 425$ nm, which is characteristic of DMFc in organic solution, and the appearance of a band at $\lambda = 779$ nm, which is characteristic of the presence of $DMFc^+$.[7]

When KI and starch were added to the aqueous phase taken from the experiments with acidic aqueous solution, the color
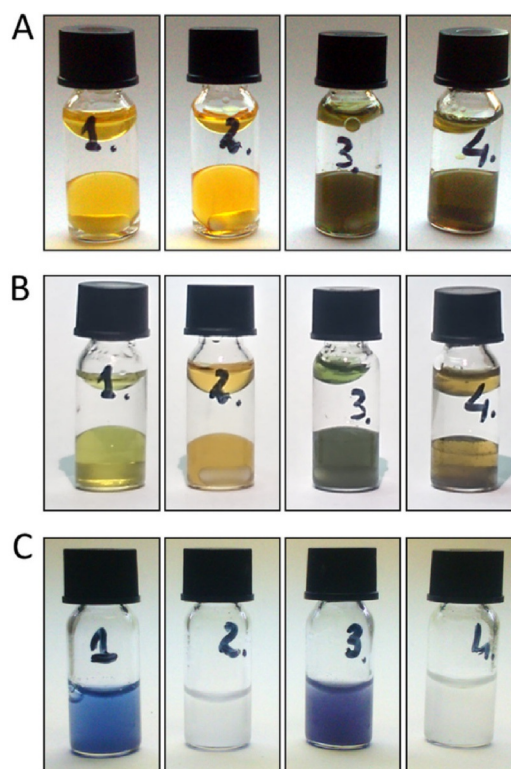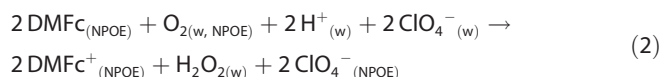

Figure 1. A, B): The results of a two-phase reaction performed in shake-flask experiments. The bottom phase consisted of DMFc (5 mmol dm^{-3}) in NPOE and the upper phase consisted of aqueous HClO$_4$ (0.1 mol dm^{-3}; flasks 1 and 3) or aqueous NaClO$_4$ (0.1 mol dm^{-3}, flasks 2 and 4). Flasks 3 and 4 also contained MoS$_2$ powder. Photographs were taken before (A) and after (B) a reaction time of 8 h. C) The aqueous phase from flasks 1–4 in B) after addition of 200 μL of a KI (0.1 mol dm^{-3}) and starch solution (10%).

changed to violet (Figure 1 C, flasks 1 and 3) due to the oxidation of iodide to triiodide by newly formed H_2O_2 and subsequent formation of a violet complex of I_3^- with starch. Additionally, formation of I_3^- by reaction with the aqueous solution was studied by using UV/Vis spectroscopy (Figure 2 B), and a characteristic peak for triiodide ($\lambda = 330$ nm) appeared in the spectrum of the yellow solution [Eq. (1)].[10]

$$3 I^- + H_2O_2 + 2 H^+ \rightarrow I_3^- + 2 H_2O \tag{1}$$
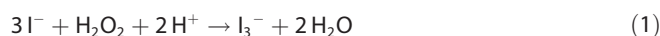
The above results indicate the generation of H_2O_2 in the following reaction [Eq. (2)]:

$$\begin{aligned} 2\,DMFc_{(NPOE)} + O_{2(w,\,NPOE)} + 2\,H^+_{(w)} + 2\,ClO_4^-_{(w)} \rightarrow \\ 2\,DMFc^+_{(NPOE)} + H_2O_{2(w)} + 2\,ClO_4^-_{(NPOE)} \end{aligned} \tag{2}$$

2.2. Voltammetry

After determining that NPOE is a suitable solvent for two-phase H_2O_2 generation, we performed voltammetric experiments with both CPE and CPE-MoS_2 electrodes. The use of a CPE with a binder of DMFc in NPOE has already been report-
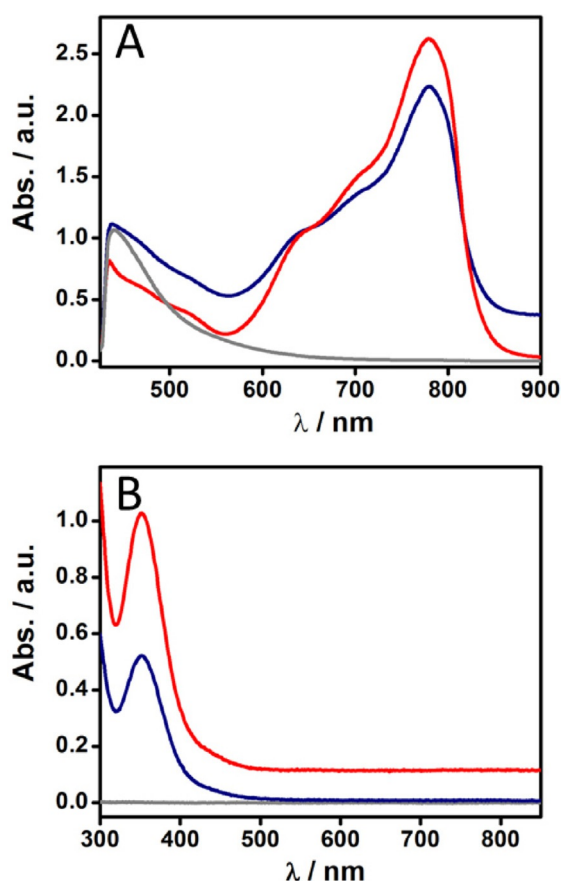
Figure 2. The UV/Vis spectra of organic and aqueous phases obtained after 8 h shake-flask experiments. A) Spectra of organic phase from flask 1 (blue) and 3 (red; see Figure 1). In the case of flask 3, MoS_2 microparticles were centrifuged. Gray line correspond to the spectrum of freshly prepared 5 mm DMFc in NPOE. B) Spectra of aqueous phase taken out flask 1 (blue) and 3 (red) after addition of KI (see Figure 1). The gray line corresponds to 0.1 m aqueous $HClO_4$.

Figure 3. Cyclic voltammograms (10 cycles) recorded for A) a CPE and B) a CPE-MoS_2 prepared with DMFc (5 mmol dm^{-3}) in NPOE immersed in aqueous NaClO$_4$ (0.1 mol dm^{-3}; blue curves) or aqueous HClO$_4$ (0.1 mol dm^{-3}; red curves). The red dotted line indicates voltammograms obtained with CPE prepared from pure NPOE. Scan rate 0.05 V s^{-1}.

ed,[35] so we focused here on the effect of MoS_2 additive on the voltammetric response of the electrode.

For this purpose, we studied ion-transfer processes across a NPOE/water interface. The voltammetric peaks recorded in perchlorate neutral and acidic solutions correspond to DMFc electrochemical redox reactions and are symmetric and stable during the subsequent cycles (Figure 3A, B). This behavior confirms that DMFc$^+$ is not transferred from NPOE to the aqueous phase during the two-phase reaction. Additive MoS_2 shifted the position of voltammogram peaks on a potential scale by a few tens of millivolts. For both CPE and CPE-MoS_2, the peak current is linearly dependent on the square root of the scan rate (Figures S1 and S2 in the Supporting Information), which indicates that MoS_2 microparticles do not change the diffusional nature of the electrochemical processes.

The voltammetry performed at this electrode in a number of aqueous solutions of salts with different anions provides a diagnostic tool for the mechanism of the electrode reaction.[35–38] In particular, it allows us to determine whether the electrogenerated DMFc$^+$ cation (here an electron acceptor) stays in the organic phase or is transferred to the aqueous phase. Clearly, the type of anion affects the position of the square wave voltam-
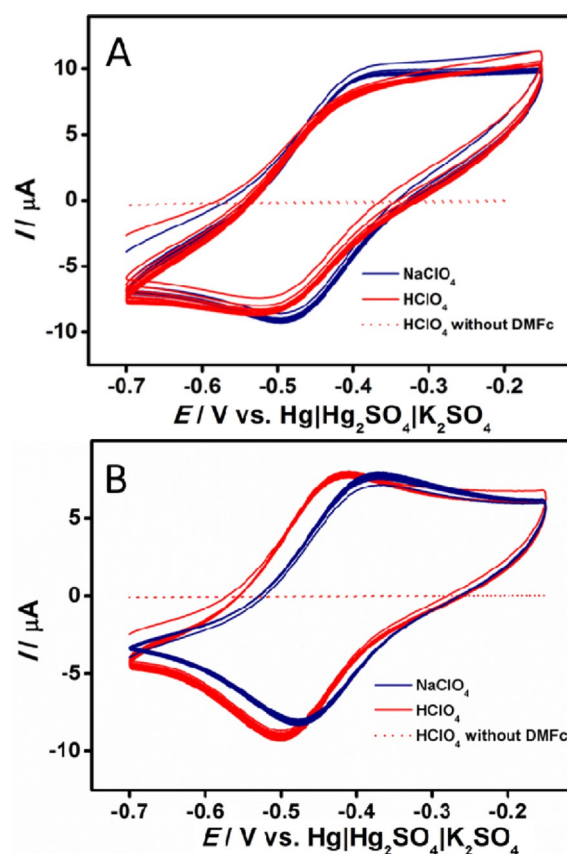
metry (SWV) peak that corresponds to the DMFc/DMFc$^+$ redox couple (Figure 4). The peak potentials are lower for more hydrophobic anions (PF$_6^-$, ClO$_4^-$, SCN$^-$), which indicates that DMFc molecules are more easily oxidized when the aqueous anions have higher affinity for the organic phase. For more hydrophilic anions (NO$_3^-$, Br$^-$, and Cl$^-$), the peak potentials are similar, which indicates that the nature of the aqueous anion does not play a role in the overall process. This effect is not affected by the presence of nonconductive MoS_2 particles in CPE. However, wider peak half-height widths are seen for CPE-MoS_2 (Table S4), which indicates the higher specific charge-transfer resistance of this electrode, as compared with CPE, because of the smaller number of percolation paths.

To compare the anion effect between CPE and CPE-MoS_2 quantitatively, one can plot the dependence of the SWV peak potential, E_p, on the standard potential of anion transfer across the NPOE/water interface, $\Delta_W^{NPOE}\phi_{An^-}^{\ominus}$. The latter parameter is a measure of how much energy the anion requires to be able to transfer from water to NPOE and is proportional to the standard Gibbs energy of transfer, $\Delta_W^{NPOE}G_{An^-}^{\ominus}$, according to Equation (3):
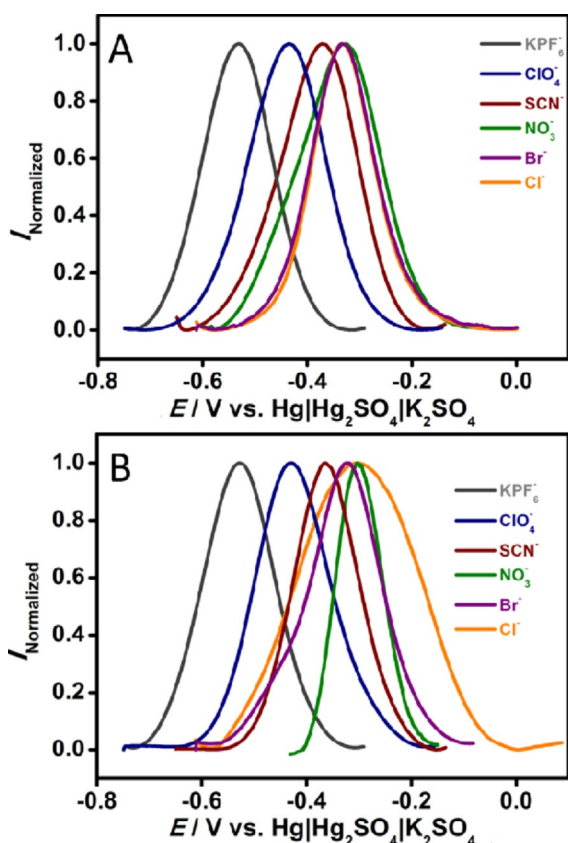
Figure 4. The effect of anion present in the aqueous phase on SWV curves obtained with A) a CPE and B) a CPE-MoS₂ prepared with DMFc (5 mmol dm^{-3}) in NPOE immersed in aqueous solutions of different electrolytes (0.1 mol dm^{-3}). Step potential: 1 mV, frequency: 8 Hz, amplitude: 50 mV.

$$\Delta_W^{NPOE}\phi_{An^-}^{\ominus} = \frac{\Delta_W^{NPOE}G_{An^-}^{\ominus}}{zF} \tag{3}$$

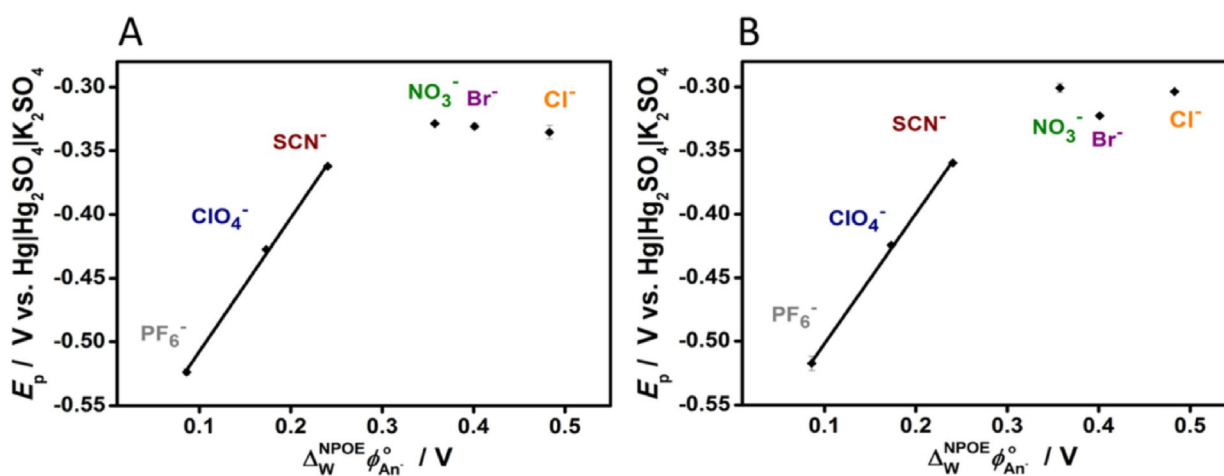in which z is the charge number of the anion and F is the Faraday constant. For the pure anion-transfer mechanism, the plot of E_p vs. $\Delta_W^{NPOE}\phi_{An^-}^{\ominus}$ is linear with a unity slope.[39] As can be seen in Figure 5, for both CPE and CPE-MoS₂ the dependence is linear with a slope close to unity for hydrophobic anions (PF₆$^-$, ClO₄$^-$, SCN$^-$), and there is virtually no dependence for hydrophilic anions (NO₃$^-$, Br$^-$, and Cl$^-$).

These results indicate that in the studied aqueous electrolytes, a gradual transition from anion insertion (for hydrophobic anions) [Eq. (4)]:

$$DMFc_{(NPOE)} + An^-{}_{(w)} \rightleftharpoons DMFc^+{}_{(NPOE)} + An^-{}_{(NPOE)} + e^-{}_{(electrode)} \tag{4}$$
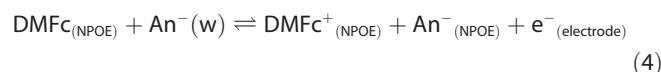
to cation expulsion (for hydrophilic anions) [Eq. (5)]:

$$DMFc_{(NPOE)} \rightleftharpoons DMFc^+{}_{(w)} + e^-{}_{(electrode)} \tag{5}$$

takes place.[35,37,40] Because the NPOE phase does not initially contain the supporting electrolyte, Reaction (4) is likely to occur at a three-phase junction between the carbon particle, NPOE, and the aqueous phase.[35] Otherwise, if the carbon particle facing the aqueous electrolyte is covered by a thin NPOE film, the electron transfer step should occur at the carbon particle–NPOE interface with simultaneous ion transfer across the NPOE–water interface. This reaction path is possible only after initial insertion of anions into the liquid binder of the CPE and usually causes the peak currents to increase in the subsequent voltammetric cycles because of the increasing concentration of the salt present in the NPOE phase next to the liquid–liquid interface.[37] Nevertheless, the stability of subsequent voltammograms (Figure 3) confirms the three-phase junction as a locus of the electrochemical processes at both CPE and CPE-MoS₂.

Regarding the two-phase reaction, the most important conclusion here is that the anion-insertion mechanism [Eq. (4)] dominates in the presence of perchlorate and the oxidized form of the electron donor does not transfer to the aqueous phase [Reaction (2)]. The presence of MoS₂ clearly does not affect this mechanism.

Figure 5. Dependence on the standard transfer potential of studied anions ($\Delta_W^{NPOE}\phi_{An^-}^{\ominus}$) of the SWV peak potential (E_p, obtained from the data presented in Figure 3) for A) CPE and B) CPE-MoS₂. The slopes in A) and B) are 1.05 and 1.02, respectively. Values of $\Delta_W^{NPOE}\phi_{An^-}^{\ominus}$ were taken from Ref. [36]. For the determination of $\Delta_W^{NPOE}\phi_{An^-}^{\ominus}$ for PF₆$^-$, see Figure S3.
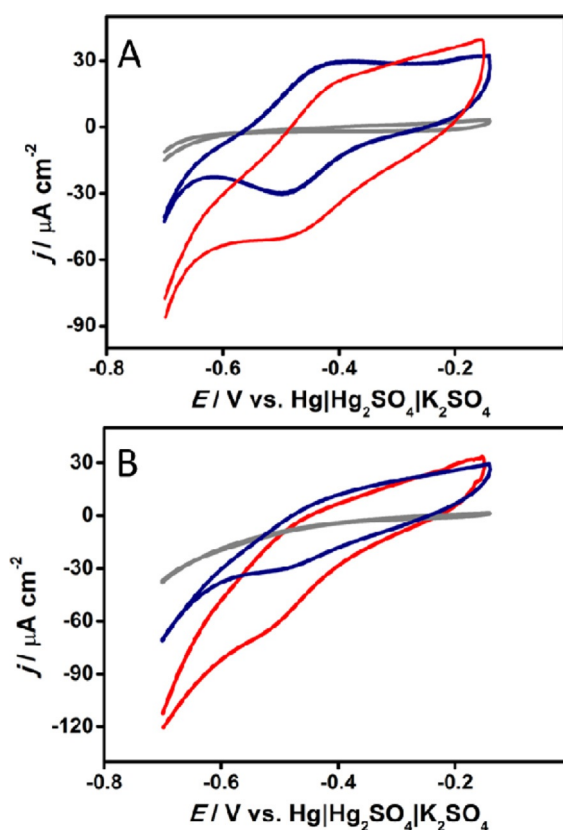
Figure 6. Cyclic voltammograms recorded for A) CPE and B) CPE-MoS$_2$ prepared with DMFc (5 mmol dm^{-3}) in NPOE, immersed in aqueous HClO$_4$ (0.1 mol dm^{-3}) saturated with O$_2$ (red curve) and saturated with Ar (blue curve). The grey curve was obtained with CPE prepared from pure NPOE in the same O$_2$ saturated solution. Scan rate 1 mV s^{-1}.

The voltammograms obtained at a slow scan rate in O$_2$- and Ar-saturated solutions show some differences (Figure 6). The anodic peak connected with oxidation of DMFc [Reaction (5)] is less developed in the presence of O$_2$ in aqueous electrolyte. A larger cathodic current compared with the anodic one indicates consumption of the electron donor in catalytic Reaction (2).[41] The cathodic peak current is clearly higher than the anodic one.

This effect is even more pronounced if MoS$_2$ microparticles are present in the CPE, however, in this case peaks are not so well developed, which is common for electrocatalytic reactions (wave-shape CV rather than peak). The absence of significant cathodic current on CPE with pure NPOE as a binder indicates the role of DMFc and MoS$_2$ as catalysts. This effect is seen only at very slow scan rates because of the sluggish kinetics of the two-phase reaction reported earlier for other molecular solvents.[12]

2.3. SECM Detection of H$_2$O$_2$

To determine directly whether H$_2$O$_2$ is formed next to the CPE, the SECM technique was applied. This was done by recording approach curves (Figure S3) by using a Pt tip polarized at a potential that corresponds to the H$_2$O$_2$ electrooxidation [Eq. (6)], here 0.6 V vs. Hg│Hg$_2$SO$_4$│K$_2$SO$_4$.[9, 42–44]
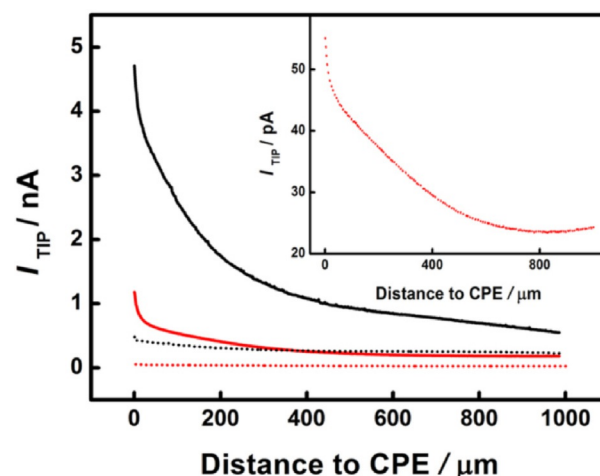

Figure 7. Comparison of H$_2$O$_2$ concentration profiles estimated from SECM approach curves (Figure S3) to CPE (red) or CPE-MoS$_2$ (black) at a Pt microelectrode tip polarized at 0.6 V in aqueous HClO$_4$ (0.1 mol dm^{-3}). DMFc (5 mmol dm^{-3}) in NPOE was used as a binder for the CPE. Solid curves were recorded when the CPE or CPE-MoS$_2$ potential was set at −0.65 V (regeneration of the electron donor), whereas dotted curves were obtained by using unbiased sample electrodes (without regeneration of the electron donor). The approaching velocity was 10 μm s^{-1}. All approach curves were recorded 5 min after the electrodes were immersed in the solution. Thin straight lines are linear regression results for distances of 150–200 μm.

$$H_2O_2 \rightarrow 2H^+ + O_2 + 2e^- \tag{6}$$

H$_2$O$_2$ concentration profiles (Figure 7) were estimated from approach curves, assuming diffusion-limiting H$_2$O$_2$ oxidation at the ultramicroelectrode (UME) disk tip [Eq. (7)]:

$$c = i_T/4nFDr_T \tag{7}$$

in which c is the analyte concentration, n is the number of electrons transferred per analyte molecule (here, 2), F is the Faraday constant (96 485 C mol^{-1}), D is the diffusion coefficient of H$_2$O$_2$ (8.8×10^{-6} cm^2 s^{-1}),[12] r_T is the tip radius (12.5 μm). Due to the fact that SECM experiments were initialized 5 min after cell assembly or sample polarization, one can assume that quasi-steady-state conditions were achieved and concentration profiles recorded at a tip translation rate of 10 μm s^{-1} are reliable. Least-square linear regression was applied to find average H$_2$O$_2$ concentration gradients within the range of 150 to 200 μm, at which feedback influence is negligible. The fluxes of H$_2$O$_2$ generated at the samples that diffused towards the aqueous bulk were calculated by using Fick's first law of diffusion. For a CPE prepared by using DMFc in NPOE, with no potential applied to it, the flux of H$_2$O$_2$ generated at the CPE surface was approximately 0.46 pmol cm^{-2} s^{-1}. This flux is almost seven times smaller than that seen at the 1,2-dichloroethane/water interface,[12] not restricted by carbon particles. No H$_2$O$_2$ was detected when the electron donor (DMFc) was absent from the carbon paste (violet curve in Figure S4), which confirms its role in the two-phase Reaction (2). However, when the CPE potential was low enough to regenerate the electron donor from DMFc$^+$ formed in Reaction (2), the flux of H$_2$O$_2$

was almost 30 times higher ($\approx 13 \, \mathrm{pmol \, cm^{-2} \, s^{-1}}$) than the value obtained when the CPE was unbiased. This indicates the electrochemical regeneration of DMFc, which results in a greater efficiency of H_2O_2 formation. This effect is much more pronounced than that observed in a CPE with a hydrophobic ionic liquid as a binder.[13]

Modification of the CPE with MoS_2 resulted in an additional increase in the flux of H_2O_2 generated at both unbiased ($\approx 4.6 \, \mathrm{pmol \, cm^{-2} \, s^{-1}}$) and biased CPEs ($\approx 81 \, \mathrm{pmol \, cm^{-2} \, s^{-1}}$). This result clearly confirms the catalytic activity of MoS_2 particles observed in the flask experiments in Figure 1B, flask 3.

Unsuccessful attempts to detect hydrogen generation at the NPOE/water interface by using methodology proposed previously[45] indicates a lack of catalytic hydrogen evolution in the studied system.

3. Conclusions

Herein, we have shown that hydrogen peroxide can be generated at the NPOE/water interface with decamethylferrocene as the electron donor. MoS_2 microparticles accelerate this reaction and their catalytic effect was observed by using cyclic voltammetry and recording SECM approach curves. By using carbon paste as a reservoir for the viscous NPOE phase, we regenerated the electron donor, which in turn resulted in an increase in the quantity of generated H_2O_2. Electrochemical studies of ion-transfer processes also revealed that addition of MoS_2 microparticles to the carbon paste does not affect the electrochemical performance of the so-obtained electrode material. A similar methodology can be applied to studies of interfacial reactions at liquid–liquid interfaces in which one of the liquid phases is viscous enough to apply as a binder in a carbon-paste electrode.

Experimental Section

Chemicals and Materials

Decamethylferrocene (DMFc; 99%, ABCR), 2-nitrophenyloctyl ether (NPOE; Fluka), $HClO_4$ (70%, Fluka), $NaClO_4$ (>99%, Fluka), $NaBF_4$ (>99.99%, Fluka), NaCl (>99%, Fluka), NaSCN (purum, Fluka), KI (pure p.a., POCh), KBr (pure p.a., POCh), KPF_6 (99%, Sigma Aldrich), KNO_3 (pure p.a. POCh), KI (pure p.a., POCh), graphite powder ($d < 20 \, \mu m$, CAS 7782-42-5, Sigma–Aldrich), MoS_2 ($\approx 6 \, \mu m$, Sigma Aldrich), starch (Sigma Aldrich), and argon gas (>99.999% Multax) were used as received. Aqueous solutions were prepared with demineralized and filtered water from ELIX system (Millipore).

Apparatus and Procedures

Flask experiments were done by filling glass vials (2 mL) with DMFc in NPOE (0.75 mL) and aqueous $HClO_4$ or $NaClO_4$ (0.75 mL). In blank experiments, pure NPOE or aqueous $NaClO_4$ were used. In other experiments, MoS_2 powder (0.5% w/v) was added to the organic phase. The samples were stirred with a magnetic bar for 8 h. For starch and iodide-based H_2O_2 detection, the aqueous phase was sampled and KI (200 μL, 0.1 mol dm^{-3}) and starch solution (10%) was added.[45]

CPEs (1.55 mm diameter) were prepared by filling glass tubes with NPOE-based carbon paste. Copper wire was inserted from the reverse to ensure electric contact. The paste was prepared by grinding DMFc (200 μL, 5 mmol dm^{-3}) in NPOE in a mortar with graphite powder (200 mg) for CPEs or graphite powder (100 mg) and MoS_2 powder (100 mg) for CPE-MoS_2. It was polished on printer paper (200 g m^{-2}) before use. For blank experiments, the same volume of pure NPOE was used.

Cyclic voltammetry and square wave voltammetry (SWV) were recorded by using a Biologic Bipotentiostat SP-300. A CPE, a graphite rod, and a $Hg/Hg_2SO_4/K_2SO_4$ electrode (Metrohm) were used as the working, counter, and reference electrodes, respectively. This reference was selected to avoid the possible contribution of Cl$^-$ oxidation to the measured oxidation current in SECM experiments. The working electrode was inserted from the bottom of the polyethylene cell so that it faced upwards during the experiments. All measurements were performed at RT ((23 ± 2)°C).

SECM experiments were carried out by using a CHI900B SECM workstation (CH Instruments). Pt microelectrodes were made by using a PC-10 micropipette puller (Narishige) to seal a Pt wire (25 μm diameter, Goodfellow, United Kingdom) into borosilicate glass capillaries polished with P2000 grit silicon carbide sand paper and 50 nm alumina slurry (Buehler). The Pt microelectrode in the aqueous phase served as the SECM probe and its position in the *x*, *y*, and *z* directions was controlled by using stepper motors.

Acknowledgements

[1] M. Méndez, R. Partovi-Nia, I. Hatay, B. Su, P. Ge, A. Olaya, N. Younan, M. Hojeij, H. H. Girault, *Phys. Chem. Chem. Phys.* **2010**, *12*, 15163 – 15171.

[2] M. A. Kamyabi, F. Soleymani-Bonoti, R. Bikas, H. Hosseini-Monfared, N. Arshadi, M. Siczek, T. Lis, *Phys. Chem. Chem. Phys.* **2015**, *17*, 32161 – 32172.

[3] Y. Xuan, X. Huang, B. Su, *J. Phys. Chem. C* **2015**, *119*, 11685 – 11693.

[4] A. Volkov, A. D. Deamer, D. Tanelian, V. Markin, *Liquid Interfaces in Chemistry and Biology*, Wiley, New York, **1998**.

[5] W. T. Hess in *Encyclopedia of Chemical Technology, Vol. 13, 4th ed.* (Eds.: Kirk-Othmer), Wiley, Hoboken, **2001**, pp. 961 – 995.

[6] G. Goor, J. Glennebergo, S. Jacobi in *Ullmann's Encyclopedia of Industrial Chemistry, Vol. 18, 7th ed.*, Wiley-VCH, Weinheim, **2012**, pp. 393 – 427.

[7] B. Su, I. Hatay, P. Y. Ge, M. Mendez, C. Corminboeuf, Z. Samec, M. Ersoz, H. Girault, *Chem. Commun.* **2010**, *46*, 2918 – 2919.

[8] P. Peljo, L. Murtomaki, T. Kallio, H.-J. Xu, M. Meyer, C. P. Gros, J.-M. Barbe, H. H. Girault, K. Laasonen, K. Kontturi, *J. Am. Chem. Soc.* **2012**, *134*, 5974 – 5984.

[9] W. Adamiak, J. Jedraszko, O. Krysiak, W. Nogala, J. Hidalgo-Acosta, H. H. Girault, M. Opallo, *J. Phys. Chem. C* **2014**, *118*, 23154 – 23161.

[10] B. Su, R. Partovi-Nia, F. Li, M. Hojeij, M. Prudent, C. Corminboeuf, Z. Samec, H. H. Girault, *Angew. Chem. Int. Ed.* **2008**, *47*, 4675 – 4678; *Angew. Chem.* **2008**, *120*, 4753 – 4756.

[11] J. Jedraszko, W. Nogala, W. Adamiak, E. Rozniecka, I. Lubarska-Radziejewska, H. H. Girault, M. Opallo, *J. Phys. Chem. C* **2013**, *117*, 20681 – 20688.

[12] W. Adamiak, J. Jedraszko, W. Nogala, M. Jonsson-Niedziolka, S. Dongmo, G. Wittstock, H. H. Girault, M. Opallo, *J. Phys. Chem. C* **2015**, *119*, 20011 – 20015.

[13] J. Jedraszko, W. Nogala, W. Adamiak, S. Dongmo, G. Wittstock, H. H. Girault, M. Opallo, *Chem. Commun.* **2015**, *51*, 6851–6853.

[14] I. Švancara, K. Vytřas, K. Kalcher, A. Walcarius, J. Wang, *Electroanalysis* **2009**, *21*, 7–28.

[15] E. Aslan, I. H. Patir, M. Ersoz, *Chem. Eur. J.* **2015**, *21*, 4585–4589.

[16] E. Aslan, I. Akin, I. H. Patir, *ChemCatChem* **2016**, *8*, 719–723.

[17] E. Aslan, I. Akin, I. H. Patir, *Chem. Eur. J.* **2016**, *22*, 5342–5349.

[18] A. N. J. Rodgers, R. A. W. Dryfe, *ChemElectroChem* **2016**, *3*, 472–479.

[19] M. D. Scanlon, X. Bian, H. Vrubel, V. Amstutz, K. Schenk, X. Hu, B. Liu, H. H. Girault, *Phys. Chem. Chem. Phys.* **2013**, *15*, 2847–2857.

[20] T. Wang, D. Gao, J. Zhuo, Z. Zhu, P. Papakonstantinou, Y. Li, M. Li, *Chem. Eur. J.* **2013**, *19*, 11939–11948.

[21] H. Huang, X. Feng, C. Du, S. Wu, W. Song, *J. Mater. Chem. A* **2015**, *3*, 16050–16056.

[22] I. Hatay, P. Y. Ge, H. Vrubel, X. Hu, H. H. Girault, *Energy Environ. Sci.* **2011**, *4*, 4246–4251.

[23] P. Y. Ge, M. D. Scanlon, P. Peljo, X. Bian, H. Vrubel, A. O'Neill, J. N. Coleman, M. Cantoni, X. Hu, K. Kontturi, B. H. Liu, H. H. Girault, *Chem. Commun.* **2012**, *48*, 6484–6486.

[24] S. Xie, X. Meng, Z. Liang, B. Li, Z. Chen, Z. Zhu, M. Li, Y. Shao, *J. Phys. Chem. C* **2008**, *112*, 18117–18124.

[25] C. Wei, A. J. Bard, M. V. Mirkin, *J. Phys. Chem.* **1995**, *99*, 16033–16042.

[26] M. Tsionsky, A. J. Bard, M. V. Mirkin, *J. Am. Chem. Soc.* **1997**, *119*, 10785–10792.

[27] M.-H. Delville, M. Tsionsky, A. J. Bard, *Langmuir* **1998**, *14*, 2774–2779.

[28] Y. Shao, M. V. Mirkin, *J. Electroanal. Chem.* **1997**, *439*, 137–143.

[29] Y. Shao, M. V. Mirkin, *J. Phys. Chem. B* **1998**, *102*, 9915–9921.

[30] C. J. Slevin, P. R. Unwin, *Langmuir* **1997**, *13*, 4799–4803.

[31] U. Schröder, J. Wadhawan, R. G. Evans, R. G. Compton, B. Wood, D. J. Walton, R. R. France, F. Marken, P. C. B. Page, C. M. Hayman, *J. Phys. Chem. B* **2002**, *106*, 8697–8704.

[32] V. A. Hernández, F. Scholz, *Electrochem. Commun.* **2006**, *8*, 967–972.

[33] J. C. Ball, F. Marken, Q. Fulian, J. D. Wadhawan, A. N. Blythe, U. Schroder, R. G. Compton, S. D. Bull, S. G. Davies, *Electroanalysis* **2000**, *12*, 1017–1025.

[34] F. Quentel, V. Mirceski, M. L'Her, *J. Phys. Chem. B* **2005**, *109*, 1262–1267.

[35] G. Shul, M. Opallo, *Electrochem. Commun.* **2005**, *7*, 194–198.

[36] F. Quentel, V. Mirceski, C. Elleouet, M. L'Her, *J. Phys. Chem. C* **2008**, *112*, 15553–15561.

[37] G. Shul, J. Sirieix-Plenet, L. Gaillon, M. Opallo, *Electrochem. Commun.* **2006**, *8*, 1111–1114.

[38] S. Komorsky-Lovrić, M. Lovrić, F. Scholz, *J. Electroanal. Chem.* **2001**, *508*, 129–137.

[39] F. Scholz, R. Gulaboski, *ChemPhysChem* **2005**, *6*, 16–28.

[40] G. Shul, W. Nogala, I. Zakorchemna, J. Niedziolka, M. Opallo, *J. Solid State Electrochem.* **2008**, *12*, 1285–1291.

[41] T. D. Chung, F. C. Anson, *J. Electroanal. Chem.* **2001**, *508*, 115–122.

[42] C. M. Sánchez-Sánchez, J. Rodriguez-López, A. J. Bard, *Anal. Chem.* **2008**, *80*, 3254–3260.

[43] Y. Shen, M. Trauble, G. Wittstock, *Anal. Chem.* **2008**, *80*, 750–759.

[44] F. Li, B. Su, F. C. Salazar, R. Partovi-Nia, H. H. Girault, *Electrochem. Commun.* **2009**, *11*, 473–476.

[45] J. Jedraszko, W. Nogala, W. Adamiak, H. H. Girault, M. Opallo, *Electrochem. Commun.* **2014**, *43*, 22–24.